Semi-Analytic Modelling of Slot Waveguides in Silicon-Organic Hybrid Mach-Zehnder Modulators

Raik Elster, Niklas Hoppe, and Manfred Berroth
Institute of Electrical and Optical Communications Engineering
University of Stuttgart
Stuttgart, Germany
raik.elster@int.uni-stuttgart.de

***Abstract*—A semi-analytic approach for modelling the distributed capacitance and the elecrooptic confinement factor of the slot waveguide in a silicon-organic hybrid Mach-Zehnder modulator using the principle of conformal mapping is presented. The results show a deviation of less than 1.3% compared with numerical field simulations.**

***Index Terms*—Mach-Zehnder modulator, silicon-organic hybrid**

I. Introduction

Mach-Zehnder modulators (MZMs) built on silicon-organic hybrid (SOH) technology are used in optical communications channels and provide efficient modulation. Organic materials with electrooptic coefficients up to $1000\,\frac{\mathrm{pm}}{\mathrm{V}}$ [1] combined with strong field confinement inside a slot waveguide, and high electric fields lead to voltage length products down to $0.41\,\mathrm{Vmm}$ and electrooptic bandwidths up to $40\,\mathrm{GHz}$ [2]. Earlier works established an equivalent circuit model based on measurements [3]. However, a more simple method for finding the optimum parameters is desired in order to save time and effort. We present a semi-analytic model to calculate the distributed capacitance, as well as the electrooptic confinement factor, for the slot waveguide with the help of conformal mapping and the Schwarz-Christoffel transformation [4]. The results are then compared with numerical field simulations performed with CST Microwave Studio's low frequency electrostatic solver.

II. Theory and Results

This work investigates the basic structure of an SOH-MZM electrode shown in Fig. 1. A slot waveguide lies between gold conductors of a coplanar waveguide. The whole structure is covered by polymethylmethacrylate (PMMA), which carries the organic material with a high electrooptic coefficient. We also compare three different silicon-on-insulator technology parameter sets: Variant 1 ($h_{\mathrm{WG}} = 250\,\mathrm{nm}$, $d_{\mathrm{BOX}} = 3\,\mathrm{\mu m}$), variant 2 ($h_{\mathrm{WG}} = 220\,\mathrm{nm}$, $d_{\mathrm{BOX}} = 2\,\mathrm{\mu m}$), and variant 3 ($h_{\mathrm{WG}} = 310\,\mathrm{nm}$, $d_{\mathrm{BOX}} = 2\,\mathrm{\mu m}$).

A. Calculation of the Slot Capacitance

For the calculation of the slot capacitance we assume the silicon rails and slabs to be perfect electric conductors due to doping. The calculation area is limited by the edges of the silicon slabs. Based on [5] the distributed capacitance below

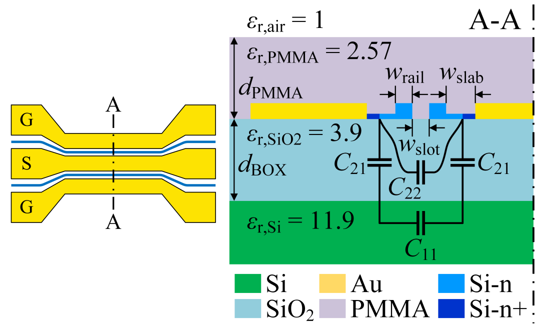

Fig. 1. Top view of a SOH-MZM electrode (left) and its cross section including symmetry axis (right). The height of the silicon rails with w_{rail} is h_{WG} and the slabs connect the rails with the electrodes. Si-n stands for moderately n-doped silicon, while Si-n+ refers to highly n-doped silicon.

the slot waveguide consists of C_{11}, C_{21}, and C_{22}. The method is modified by replacing the terms $(\varepsilon_i - 1)$ with the dielectric permittivity ε_i due to the adapted calculation of C_{11}. C_{21} is found with the calculation of one quadrant for a shielded strip line [6]. C_{22} remains unmodified. C_{11} is then defined as

$$C_{11} = \frac{\varepsilon_{\mathrm{Si}}}{2\varepsilon_{\mathrm{SiO_2}}}\left[\frac{1}{\varepsilon_{\mathrm{SiO_2}}\mathrm{K}(k_1')/\mathrm{K}(k_1) - 2C_{22}} - \frac{1}{C_{21}}\right]^{-1} \quad (1)$$

where $\mathrm{K}(k)$ is the complete elliptic integral of the first kind, $k_1 = \sin(\pi\, w_{\mathrm{slot}}/(2w_{\mathrm{slot}} + 4(w_{\mathrm{rail}} + w_{\mathrm{slab}})))$, and $k_1' = \sqrt{1-k_1^2}$. In addition, the capacitance above the slot waveguide comprises contributions from the PMMA with a finite height d_{PMMA} and from the air above with infinite height. Fig. 2 shows the initial complex planes in the z domain. Finding the right mapping function is crucial for accurate results. The derivation, which defines the Schwarz-Christoffel transformation from the z plane to the w plane, is for Fig. 2(a)

$$\frac{\mathrm{d}z}{\mathrm{d}w} = \sqrt{\frac{(w^2-w_2^2)(w^2-w_3^2)}{(w^2-w_1^2)(w^2-w_4^2)}} \quad (2)$$

and for Fig. 2(b)

$$\frac{\mathrm{d}z}{\mathrm{d}w} = \sqrt{\frac{(w-w_4)(w-w_5)}{(w-w_1)(w-w_2)(w-w_3)(w-w_6)}}. \quad (3)$$

The coefficients $w_i = w(z_i)$ are calculated numerically. The mapping from (2) leads to a symmetric coplanar stripline in the w plane and from (3) to an asymmetric coplanar stripline in the w plane, respectively, both with infinitely thin electrodes. The capacitance of both electrode configurations is then calculated

978-1-6654-7899-1/22/$31.00 ©2022 IEEE

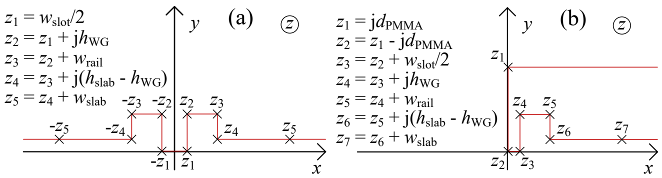

Fig. 2. The cross section of the slot waveguide transferred into a coordinate system (z domain). (a) shows the initial polygon for the contribution of the air and (b) shows the initial polygon for the PMMA layer. Due to the finite height in (b) only the right side with an electric wall between z_1 and z_2 is mapped.

and added up based on known methods of partial capacitance calculation [6].

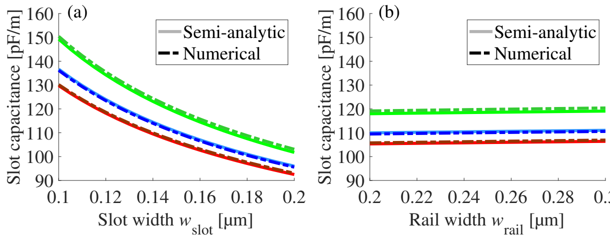

Fig. 3. Semi-analytic and numerical values of the slot capacitance of variant 1 (blue), variant 2 (red), and variant 3 (green) with (a) $w_{\mathrm{rail}} = 250\,\mathrm{nm}$ and (b) $w_{\mathrm{slot}} = 150\,\mathrm{nm}$. The slot capacitance consists of the contributions above and below the slot waveguide.

Fig. 3 shows a maximum deviation between numerical simulation and semi-analytic calculation of less than 1.3%. The semi-analytic calculation time per data point is below $4\,\mathrm{s}$, while the numerical simulation time is around $4\,\mathrm{min}$ with around $4 \cdot 10^5$ tetrahedrons and a maximum mesh edge length of about $300\,\mathrm{nm}$.

B. Calculation of the Electrooptic Confinement Factor

The electrooptic confinement factor Γ_{eo} describes the overlap between the electric field of the optical mode guided by the slot waveguide and the electric field $E_{\mathrm{appl}}(x, y)$ of the applied electrode voltage V. The modulation efficiency is linear proportional to Γ_{eo}, which is defined as [7]

$$\Gamma_{\mathrm{eo}} = \frac{n_{\mathrm{PMMA}}\, w_{\mathrm{slot}}}{2P_{\mathrm{opt}}\, Z_0\, V} \iint\limits_{PMMA} \frac{|E_{\mathrm{appl}}(x,y)|^2}{\overline{|E_{\mathrm{appl}}|_{\mathrm{slot}}}} \cdot |E_{\mathrm{opt}}(x,y)|^2 \cos(\vartheta(x,y))^2 \mathrm{d}x\mathrm{d}y \tag{4}$$

where E_{opt} is the electric field of the guided mode in the slot waveguide, P_{opt} is the mode power, Z_0 is the free space characteristic impedance, and $\vartheta(x, y)$ is the angle between $E_{\mathrm{appl}}(x, y)$ and $E_{\mathrm{opt}}(x, y)$. By shifting the position of z_1 in Fig. 2(a) to the position of the magnetic wall $(w_{\mathrm{slot}} + \mathrm{j}h_{\mathrm{WG}})/2$, it's possible to calculate $E_{\mathrm{appl}}(x, y)$ accurately. After mapping the slot waveguide's cross section from the z domain over the intermediate w domain into a rectangle, it is easy to solve the Poisson's equation for the electric potential, which is mapped back to the initial z domain. The electric potential of the upper half of the slot is mirrored into the lower half due to the magnetic wall at $y = h_{\mathrm{WG}}/2$. E_{appl} is then calculated by applying the gradient to the electric potential. In the end, the result is used to compute Γ_{eo} with E_{opt}, which is simulated in Fimmwave. Fig. 4 shows the field profiles and verifies the accuracy of the proposed method, since the profiles match well.

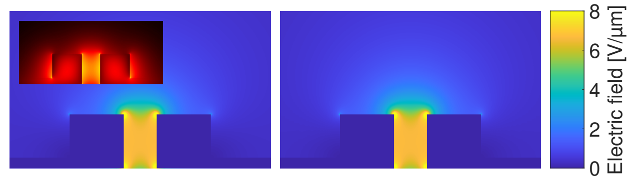

Fig. 4. Numerically simulated (left) and semi-analytically calculated (right) $|E_{\mathrm{appl}}|$ at $V = 1\,\mathrm{V}$, $w_{\mathrm{slot}} = 150\,\mathrm{nm}$, and $w_{\mathrm{rail}} = 250\,\mathrm{nm}$. The inset shows the electric field profile $|E_{\mathrm{opt}}|$.

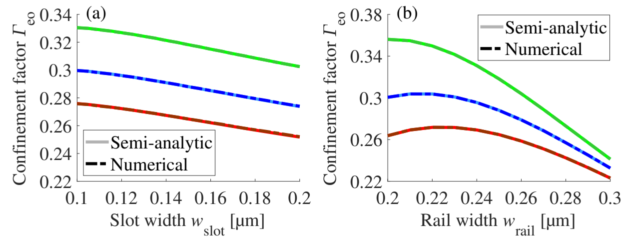

Fig. 5. Semi-analytic and numerical values of Γ_{eo} of variant 1 (blue), variant 2 (red), and variant 3 (green) with (a) $w_{\mathrm{rail}} = 250\,\mathrm{nm}$ and (b) $w_{\mathrm{slot}} = 150\,\mathrm{nm}$.

The results of Γ_{eo} in Fig. 5 show a maximum deviation of less than 0.1%. The numerical simulation time per data point is approximately $10\,\mathrm{min}$ with around $9 \cdot 10^5$ tetrahedrons and a maximum mesh edge length of $55\,\mathrm{nm}$, while the semi-analytic calculation time is around $90\,\mathrm{s}$.

III. Conclusion and Outlook

We presented an efficient semi-analytic method for calculating the capacitance of a slot waveguide as well as of the electrooptic confinement factor. The proposed method provides accurate results with a maximum deviation of 1.3% compared to numerical field simulations. By using the proposed semi-analytic method the computation time may be significantly reduced.

Acknowledgment

This work is funded by the Deutsche Forschungsgemeinschaft (DFG) under grant no. BE 2256/36-1.

References

[1] H. Xu *et al.*, "Electro-Optic Activity in Excess of 1000 pm V^{-1} Achieved via Theory-Guided Organic Chromophore Design," *Adv. Mater.*, vol. 3, no. 45, pp. 2104174, Sep. 2021.

[2] C. Kieninger *et al.*, "Silicon-organic hybrid (SOH) Mach-Zehnder modulators for 100 GBd PAM4 signaling with sub-1 dB phase-shifter loss," *Opt. Express*, vol. 28, no. 17, pp. 24693–24707, Aug. 2020.

[3] H. Zwickel *et al.*, "Verified equivalent-circuit model for slot-waveguide modulators," *Opt. Express*, vol. 28, no. 9, pp. 24693–24707, Apr. 2020.

[4] C. Nguyen, "The Schwarz-Christoffel Transformation," *Analysis Methods for RF, Microwave, and Millimeter-Wave Planar Transmission Line Structures*, 1st ed. New York, NY, USA: Wiley, 2000, ch. 5.3, pp. 95–98.

[5] S. Gevorgian, H. Berg, H. Jacobsson, and T. Lewin, "Basic Parameters of Coplanar-Strip Waveguides on Multilayer Dielectric/Semiconductor Substrates, Part 2: Low Permittivity Superstrates," *IEEE Microw. Magazine*, vol. 4, no. 3, pp. 59–78, Sep. 2003.

[6] C. Nguyen, "Applications of the Schwarz-Christoffel Transformation in Transmission Line Analysis," *Analysis Methods for RF, Microwave, and Millimeter-Wave Planar Transmission Line Structures*, 1st ed. New York, NY, USA: Wiley, 2000, ch. 5.4, pp. 106–111.

[7] C. Kieninger *et al.*, "Ultra-high electro-optic activity demonstrated in a silicon-organic hybrid modulator: supplementary material," *Optica*, vol. 5, no. 6, Jun. 2018.